https://doi.org/10.5194/egusphere-2022-1402
Preprint. Discussion started: 21 December 2022

Evaluation of total ozone measurements from Geostationary Environmental Monitoring Satellite (GEMS)

Kanghyun Baek[1], Jae Hwan Kim[1], Juseon Bak[2], David P. Haffner[3], Mina Kang[4], Hyunkee Hong[5]

[1] Department of Atmospheric Science, Pusan National University, Busan, Republic of Korea
[2] Institute of Environmental Studies, Pusan National University, Busan, Republic of Korea
[3] NASA Goddard Space Flight Center, Greenbelt, MD 20771, USA
[4] Department of Atmospheric Science and Engineering, Ewha Woman's University, Seoul, Republic of Korea.
[5] National Institute of Environmental Research, Incheon, Republic of Korea.

Correspondence to: Jae Hwan Kim (jaekim@pusan.ac.kr)

Abstract. As all life on earth depends crucially on atmospheric ozone, low earth orbiting (LEO) satellites have been used to monitor atmospheric ozone to reduce its impact on the environment and public health. The continued interest in air pollution and stratospheric ozone variability has motivated the development of a geostationary environmental monitoring satellite (GEMS) for hourly ozone monitoring. This paper provides the atmospheric science community with the world's first assessment of GEMS total column ozone (TCO) retrieval performance and diurnal ozone variation. The algorithm used for GEMS is a more advanced version of its predecessor, the TOMS-V8 algorithm. In addition to calculating total ozone, the algorithm has the advantage of providing ozone profile and retrieval error information. To assess the performance of the GEMS algorithm, the hourly GEMS total ozone was compared with ground-based measurements from four Pandora instruments and other satellite platforms from TROPOMI and OMPS. A high correlation of 0.91 or more with GEMS and Pandora TCO at Seoul, Busan, and Yokosuka but a low correlation of 0.83 at Ulsan, which is significantly smaller than at other sites. Root-mean-squared error (RMSE) showed satisfactory small values, with the lowest RMSE of 2.06 DU. Positive mean biases (MBs) were observed at all sites. This agreement suggests that the GEMS hourly ozone monitoring allows for continuous updates about stratospheric ozone and its related atmospheric changes. The quantitative comparison of GEMS TCO data with TROPOMI and OMPS TCO data shows a high correlation coefficient greater than 0.98 and a low RMSE of less than 1.8 DU over clear sky conditions. GEMS TCO underestimates by - 0.14 % (0.4 DU) with a standard deviation of 2.0 % relative to TROPOMI and overestimates by + 0.1 % (0.3 DU) with a standard deviation of 2.3 % relative to OMPS. It shows that the GEMS TCO agrees very well with the TROPOMI and OMPS TCO. The results are a meaningful scientific advance by providing the first validated, hourly UV ozone retrievals from a satellite in geostationary orbit. This experience can be used to advance research with future geostationary environmental satellite missions, including incoming TEMPO and Sentinel-4.

https://doi.org/10.5194/egusphere-2022-1402
Preprint. Discussion started: 21 December 2022

1 Introduction

Stratospheric ozone is responsible for absorbing the sun ultraviolet (UV) radiation, protecting the Earth's surface from harmful UV rays. Ozone in the troposphere is a toxic air pollutant that affects human health via harmful respiratory and cardiovascular effects, and negatively affects vegetation growth (Crutzen, 1979; Jacob et al., 1999). Global ozone monitoring is therefore essential for both public health and environmental protection to provide valuable information about the state of the atmosphere and identify areas where public action is needed to reduce impacts on human health and the environment (Engel et al., 2018; Scientific Assessment of Ozone Depletion, 2014).

Satellite remote sensing is a powerful tool for monitoring atmospheric ozone with high spatial and temporal coverage of global observations (Fishman et al., 2008; Fishman and Larsen, 1987). Global ozone monitoring by Total Ozone Monitoring Spectrometer (TOMS) aboard the Nimbus-7 satellite in 1978 was the first mission dedicated to creating detailed maps of atmospheric ozone from space (Bhartia et al., 1996). Since then, the Global Ozone Monitoring Experiment (GOME) (ESA 1995), SCanning Imaging Absorption spectroMeter for Atmospheric CHartographY (SCIAMACHY) (Bovensmann et al., 1999), Ozone Monitoring Instrument (OMI) (Levelt et al., 2006), Ozone Mapping and Profiler Suite Nadir Mapper (OMPS) (Flynn et al., 2014), and TROPOspheric Monitoring Instrument (TROPOMI) (Veefkind et al., 2012), which all built on the success of TOMS, have provided a continuous and consistent mapping of atmospheric ozone.

The continued interest in air pollution and stratospheric ozone variability has motivated the development of new satellite missions with improved capabilities for hourly monitoring of atmospheric composition. The geostationary Air Quality (Geo-AQ) constellation missions such as Geostationary Environmental Monitoring Satellite (GEMS), Sentinel-4, and Tropospheric Emissions: Monitoring of Pollution (TEMPO) were designed to provide high-quality measurements of atmospheric composition throughout the day from geostationary orbit (Ingmann et al., 2012; Zoogman et al., 2017; Kim et al., 2020). These new missions will provide more accurate and timely information about air quality and stratospheric ozone for supporting air quality forecasts and policy making. The Geo-Kompsat-2B satellite carrying the GEMS sensor was the first mission of the Geo-AQ constellation, which was launched on 18 February 2020 (Kim et al., 2020). GEMS is a UV–visible spectrometer that measures direct solar irradiance and radiance backscattered from the Earth's surface and atmosphere covering the Asia-Pacific region (Kim et al., 2020).

Since GEMS is the first Geo-AQ mission, it is necessary to introduce the algorithm process and new data products to provide information for users. Here we focus on the GEMS total ozone (O3T) algorithm for retrieving total column ozone (TCO) from GEMS Level-1B (L1B) radiance spectra, and validation of these data using ground-based Pandora TCO measurements, and other satellite TCO measurements from OMPS and TROPOMI. The GEMS-O3T algorithm has several improvements over previous algorithms, such as the use of a new look-up table (LUT), simple Lambert equivalent reflectivity (LER) model, and correction for spectral dependence of LER, and the use of GEMS Level-2 (L2) Cloud product. The algorithm is now flexible enough to handle additional wavelengths and more readily employ different sources of a priori profile information without

https://doi.org/10.5194/egusphere-2022-1402
Preprint. Discussion started: 21 December 2022

significant changes to the design of the algorithm. The GEMS-O3T algorithm also uses the optimal estimation method (OEM) to make error analysis more accessible and robust.

This paper consists of five Sections: Section 2 describes the GEMS instrument and Level-1B data; Section 3 explains the differences and advantages of the GEMS algorithm from its predecessor, the TOMS algorithm; Section 4 discusses the results of retrieval characteristics and error analysis; Section 5 presents the validation results of the new TCO product with respect to ground-based Pandora TCO measurements and other satellite TCO measurements from OMPS and TROPOMI; Section 6 discusses the impact of the new algorithm on global TCO observations, and is followed by a conclusion in Section 7.

2. Data and Method

2.1 The GEMS Mission

GEMS is a UV-visible spectrometer developed for Korea's next-generation geostationary multi-purpose satellite program, which consists of two satellites, Geo-Kompsat-2A (GK-2A) and Geo-Kompsat-2B (GK-2B). They are collocated at 128.2 E over the equator. The GK-2A satellite is equipped with an Advanced Meteorological Imager (AMI) to provide high-resolution images of the Earth's surface and atmosphere for weather forecasting, while GK-2B has two payloads: one with the GEMS sensor to monitor the atmospheric composition and air quality, and another with Geostationary Ocean Color Imager (GOCI)-II to monitor ocean color.

GEMS is designed to use the same optical path for direct solar radiation and radiance backscattered from the Earth's surface and atmosphere. Using the same optical path for solar irradiance and radiance backscattered from Earth has several benefits. First, it minimizes calibration uncertainty in algorithms using the ratio of radiance to solar irradiance because sensor errors common to the radiance and irradiance measurements cancel. The measured light passes through the same calibration assembly and scan mirror, telescope, spectrometer, and detectors, which minimizes the possibility of inconsistency between measurements. However, a diffuser is used for solar irradiance measurements, and is located in front of the scan mirror, and introduces a source of calibration error that does not cancel in the radiance to irradiance ratio. The magnitude of this error is difficult to quantify and requires both in-flight calibration measurements and theoretical calculations. We will discuss the impact of this error on retrieval and how to correct it in Section 4.

GEMS measures Earth radiance in the 300-500 nm wavelength range with a high spectral sampling of 0.2 nm and spectral resolution of 0.6 nm. The spatial resolution of the instrument is 3.5 km × 7 km over Seoul, and the overall field of regard (FOR) is from 5◦ S to 45◦ N latitude and between 75 ◦E to 145 ◦E longitude every hour from 09:00 to 17:00 Korea Standard Time (KST). Solar irradiance is measured over the same wavelength range once per day in the nighttime darkness. The incident light from the telescope is dispersed onto a single two-dimensional charge-coupled device (CCD), which has 1033 spectral pixels and 2048 pixels in the spatial dimension. A two-axis mirror scans from east to west with a fixed north-south field of view, during 30-minute observation periods which collect measurements across the entire FOR

https://doi.org/10.5194/egusphere-2022-1402
Preprint. Discussion started: 21 December 2022

2.2 The GEMS algorithm

A major objective of this study was to obtain total ozone data from geostationary orbit for the first time using the UV spectrum. The GEMS-O3T algorithm was developed based on the well-researched NASA TOMS algorithm, which is the oldest and most proven method of satellite total ozone retrieval algorithms developed by Dave and Mateer (1967). Since several others have documented earlier versions of the TOMS algorithm over a half-century of development (Bhartia and Haffner, 2012; Bhartia, 2002; Dave and Mateer, 1967; Haffner et al., 2015; Haffner et al., 2022; Klenk et al., 1982; Mcpeters et al., 1996), the important goals of using the TOMS algorithm for GEMS is to obtain the most stable and reliable total ozone output. Because the TOMS algorithm was only applied to total ozone retrievals from a sun-synchronous orbiting satellite, we conducted a series of studies to improve the total ozone data quality with the GEMS-O3T algorithm. The flowchart represents the total ozone retrieval process from the improved GEMS-O3T algorithm in Figure 1. The algorithm consists of two main components: a forward model that calculates the top of atmosphere (TOA) radiance and an inverse model that derives total ozone from the measured radiance.

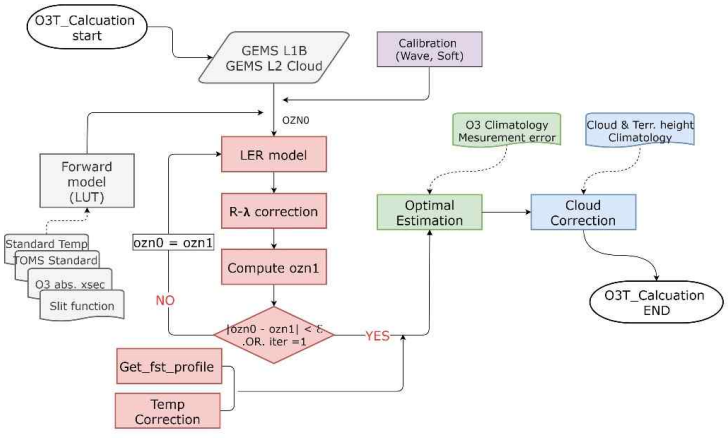

Figure 1. Flowchart of GEMS total ozone retrieval algorithm.

2.2.1 Forward model

The radiance in the six wavelengths (312.5, 317.34, 331.02, 340, and 380 nm) observed from the satellite as reflected by the atmosphere and a reflecting surface is calculated by the VLIDORT radiative transfer model (RTM) (Spurr, 2008). We used a pre-calculated lookup table since it is very time-consuming to perform the VLIDORT calculations online. The pre-calculated

https://doi.org/10.5194/egusphere-2022-1402
Preprint. Discussion started: 21 December 2022

radiances are obtained at different solar zenith angles, satellite viewing angles, and reflecting surface conditions (land/ocean, clouds, and aerosols) for 21 ozone profiles that vary with latitude band and total ozone amount (Wellemeyer et al., 1997). The surface underlying satellite viewing geometry is assumed to have the simple Lambert equivalent reflectivity (SLER) which treats surfaces, clouds, and aerosols as Lambertian reflectors at surface pressure (Ahmad, 2004). VLIDORT calculates radiances taking into account polarized Rayleigh scattering and the gas absorption (e.g., O_3 and O_4) with temperature-dependent gaseous absorption cross sections. This study used the BDM ozone absorption cross-section (Daumont et al., 1992; Brion et al., 1993; Malicet et al., 1995) and TOMS standard ozone profiles (Wellemeyer et al., 1997). VLIDORT is also used when calculating the look-up-table (LUT) for Jacobians, which are needed to perform the retrieval using optimal estimation. We used a single US standard temperature profile to optimize the table size for radiances and Jacobians. Calculated radiances are then adjusted using a zonal mean temperature climatology via a temperature correction in the algorithm.

2.2.2 Inverse Model

An inverse model in the GEMS-O3T algorithm is a mathematical tool that helps to convert the measured radiance into geophysical parameters, such as total ozone and ozone profile. The model proceeds in three steps. In Step 1, the reflectivity is derived at 380 nm, then corrected by the method suggested by Dave (1978), followed by the first guess estimate of ozone with 317.34 nm, and finally, residuals and jacobians are calculated. Step 2 is a straightforward implementation of an optimal estimation method to estimate the ozone profiles using inputs derived in Step 1 and a set of radiances (312, 317, and 331 nm) and *a priori* ozone profiles and their error covariance matrix. This process, which is not present in the TOMS-V8 algorithm, is the core of the GEMS-O3T algorithm because it provides the error amount for retrieved total ozone and the degree of freedom that shows the independent vertical information of the ozone profile. The correction for clouds and terrain height is made in the final process of Step 3.

Step 1 process starts with the computation of reflectivity using the measured BUV radiance at 380 nm based on the simple Lambert Equivalent reflectivity (SLER) model. The initial assumptions are that the spectral dependence of reflectivity (R) is zero (i.e., $dR/d\lambda = 0$). However, this assumption can no longer be valid in the presence of absorbing aerosol, sea glint, and clouds ($dR/d\lambda \neq 0$). The algorithm accounts for radiative effects of aerosols and surface reflectance by using the calculated spectral slope of $dR/d\lambda$ obtained from reflectivity at 340 nm and 380 nm with negligible ozone absorption cross-sections in Eq. (1).

$$R = R_{380} + \frac{dR}{d\lambda}(\lambda_{317} - \lambda_{380}) \quad (1)$$

This calculation updates the estimated reflectivity (R) derived after each iteration proposed by Dave (1978). However, in the presence of high amounts of UV-absorbing aerosols, $dR/d\lambda$ cannot be linear and results in a significant error in the derived reflectivity. This data is flagged during the quality control process. The dependence of the backscattered radiance on ozone is

https://doi.org/10.5194/egusphere-2022-1402
Preprint. Discussion started: 21 December 2022

approximately exponential. A quantity called the N-value is defined to reduce the dynamic range of the total ozone dependence (Klenk et al., 1982). The N-value is defined as:

$$N = -100 \log_{10} \frac{I}{F} \quad (2)$$

where F is the extraterrestrial solar irradiance. The amount of total ozone is determined when the measured N-value ($\boldsymbol{N_m}$) at 317 nm is equal to the calculated one ($\boldsymbol{N_c}$) with the total ozone amount corresponding to the TOMS standard ozone profile at a given satellite viewing geometry, solar zenith angle, surface reflectivity, and surface pressure (Bhartia and Wellemeyer 2002). The interpolation entails using three to ten ozone profiles, each with a different range of total ozone amounts for latitude. Therefore, the ozone profile shape corresponding to the retrieved total ozone is obtained by this process.

The OEM approach proposed by Roger (2000) is applied in step 2 to retrieve a coarse ozone profile, estimated from a set of radiances at three wavelengths with different amounts of ozone absorption (312.34, 317.35, and 331.06 nm) using a priori profiles and their error covariance matrices. The use of optimal estimation allows smooth transition between the use of the different wavelengths, and thereby eliminates the discontinuities associated with TOMS ozone distribution that occurs when the solar angle is large. Optimal estimation also provides information about total ozone retrieval error, degree of freedom, averaging kernel and column weighting kernel (CWK, w_k):

$$\hat{\boldsymbol{x}} = \boldsymbol{x_a} + \mathbf{S_a}\boldsymbol{K}^T(\boldsymbol{K}\mathbf{S_a}\boldsymbol{K}^T + \boldsymbol{S_e})^{-1}[(\boldsymbol{N_m} - \boldsymbol{N_1}) + \boldsymbol{K}(\boldsymbol{x_1} - \boldsymbol{x_a})];$$
$$\mathbf{G} = \mathbf{S_a}\boldsymbol{K}^T(\boldsymbol{K}\boldsymbol{S_a}\boldsymbol{K}^T + \mathbf{S_e})^{-1};$$
$$\mathbf{A} = \mathbf{G}\boldsymbol{K};$$
$$\hat{\mathbf{S}} = \mathbf{S_a} - \mathbf{S_a}\boldsymbol{K}^T(\boldsymbol{K}\mathbf{S_a}\boldsymbol{K}^T + \mathbf{S_e})^{-1}\boldsymbol{K}\boldsymbol{S_a} \quad (3)$$

where $\hat{\boldsymbol{x}}$ is the optimized ozone profile consisting of 11 Umkehr layers. The pressure at the bottom of these layers decreases by a factor of 2 starting from the mean sea-level pressure (1013.25 hPa) to 0.99 hPa. The top layer goes from 0.99 hPa to infinity. $\boldsymbol{x_l}$ is the ozone profile retrieved in Step 1. The $\boldsymbol{x_a}$ is the a-priori ozone profile obtained from ML climatological profiles (McPeters and Labow, 2012) consisting of 12-month and 18 latitudinal bands with 10-degree intervals from 90° S to 90° N. The $\mathbf{S_a}$ is a-priori error covariance matrix (11 × 11 covariance matrix) derived from the ML climatological profile, where correlation is limited to one layer from the diagonal entry. $\boldsymbol{N_m}$ is the measurement radiance vector consisting of three elements from 312, 317, and 331 nm, and $\boldsymbol{N_1}$ is the N-value calculated from $\boldsymbol{x_1}$. $\mathbf{S_e}$ is the measurement error covariance matrix, and is assumed to be a diagonal matrix where the elements are the squares of the assumed measurement errors. We assume the measurement error of 0.12 % according to GEMS SNR corresponding to 320 nm is 720. K is the Jacobian matrix, defined as $\boldsymbol{dN_j/dx_i}$ for each layer i and wavelength j, representing partial derivatives of the forward model to the ozone. The gain matrix, **G**, measures how sensitive the retrieved profile is to measurement errors, and the averaging kernel matrix, **A**, provides the sensitivity of the retrieval to a change in true ozone profile and a vertical resolution of the retrieved profile. The covariance

https://doi.org/10.5194/egusphere-2022-1402
Preprint. Discussion started: 21 December 2022

matrix $\hat{S}$ measures the degree of error in the retrieved ozone profile. It contains the measurement and smoothing errors propagated through the **G** and **A** matrices, respectively.

The total ozone obtained from Step 2 assumes that the reflecting surface is at sea level. If the surface is at a different elevation or a cloud is present, we must account for that in the total ozone calculation. After adjusting the column weighting kernel (w_l) for the profile used, the final Step 3 total ozone is calculated by subtracting the amount of ozone corresponding to the difference between the topography (or cloud) height and the ground surface from the Step 2 total ozone. Since the ozone column below the cloud pressure (p_c) is relatively small, we use a relatively simple method to correct it. If reflectivity (R) from 380 nm is less than 0.05 (R_s) or snow or ice is present, no cloud is assumed. If R is greater than 0.4 (R_c), we assume the entire pixel is covered with clouds. For $R_s < R < R_c$, the pixel was assumed to be partial cloud cover, and the cloud fraction was determined by equation (4) as follows:

$$f_c = (R - R_s)/(R_c - R_s). \quad (4)$$

We assume that this fraction (f_c) is approximately the fraction of the measured radiance signal reflected by clouds within the instrument field-of-view. We first estimate the ozone between the cloud and terrain pressure in each layer l, and then set the (w_l) in layers below p_c to zero in equation (5)

$$\boldsymbol{x}_l^* = \hat{\boldsymbol{x}}_l(1 - f_c) + \boldsymbol{x}_{a,l} f_c,$$
$$\boldsymbol{w}_l^c = \boldsymbol{w}_l(1 - f_c), \quad (5)$$

where $\hat{\boldsymbol{x}}_l$ and $\boldsymbol{x}_{a,l}$ are the ozone amount in layer l of the profile obtained from step 2 and from a priori profile respectively. Then, the correction to the total column is obtained by

$$\delta\Omega = \sum_{l=0}^{l_{pc}} \boldsymbol{x}^*{}_l\,(1 - \boldsymbol{w}_l^c) - \hat{\boldsymbol{x}}_l\,(1 - \boldsymbol{w}_l^c). \quad (6)$$

3. Results and Discussion

3.1 GEMS hourly total ozone distribution

The GEMS sensor onboard a geostationary satellite has the advantage of measuring ozone over current Low Earth Orbiting (LEO) satellite sensors because it provides hourly observations throughout the data, which helps to improve our understanding of ozone. To assess the performance of the GEMS total ozone algorithm, the hourly GEMS total ozone on 29 March 2021 is shown in Figure 2. This figure shows the eight hourly GEMS total ozone measurements from 09 Korea Standard Time (KST) to 16 KST. Because GEMS measures backscattered UV radiation when the solar zenith angle is not large, daytime hourly observation time and area vary depending on the season (NIER, 2020). Figure 2(a) shows the hemisphere east (HE) mode at 9:00 KST, Figure 2(b) shows the hemisphere Korea (HK) mode at 10:00-11:00 KST, Figure 3(c)-(d) shows the full central

https://doi.org/10.5194/egusphere-2022-1402
Preprint. Discussion started: 21 December 2022

(FC) mode at 11:00-12:00 KST, and Figure 2(e)-(h) shows the full west (FW) mode at 13:00-16:00 KST. The GEMS observation usually takes 30 minutes, running from 15-minutes before the hour to 15-minute after the hour.

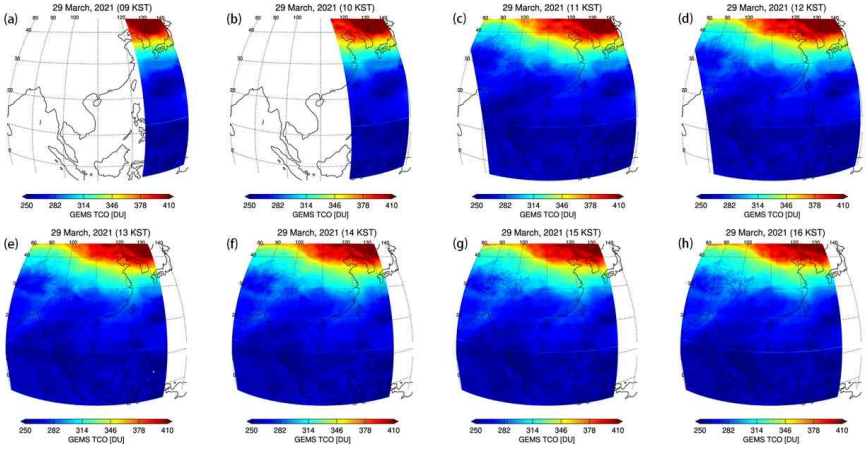

Figure 2. Hourly GEMS total ozone distribution on 29 March 2021.

The total ozone distribution ranging from 250 to 400 DU shows a typical distribution in March: High values at high latitudes, followed by a sharp decrease in the middle latitudes and gradually decreasing toward the equator. Because the scale bar is so large, changes in hourly values are not clearly seen. This GEMS hourly ozone monitoring allows for continuous updates about stratospheric ozone and its related atmospheric changes. It can also provide information about how the situation may develop in future hours.

Figure 3 compares the hourly GEMS TCO with Pandora TCO observed over eight ground sites and satellite TCO for three consecutive days from 29 to 31 March 2021. The hourly total ozone distribution in Figure 3 showed significant diurnal ozone changes of up to 40 DU. This indicates that the ozone undergoes significant diurnal change primarily due to changes in stratospheric ozone, and is evidence of why hourly ozone monitoring is important to track dynamic ozone changes. Pandora TCO varies considerably over time, and the diurnal variation of GEMS is in good agreement with that of Pandora. The GEMS data for diurnal ozone change offers advantages over TROPOM (blue) and OMPS (green) ozone data, which are observed once per day.

https://doi.org/10.5194/egusphere-2022-1402
Preprint. Discussion started: 21 December 2022

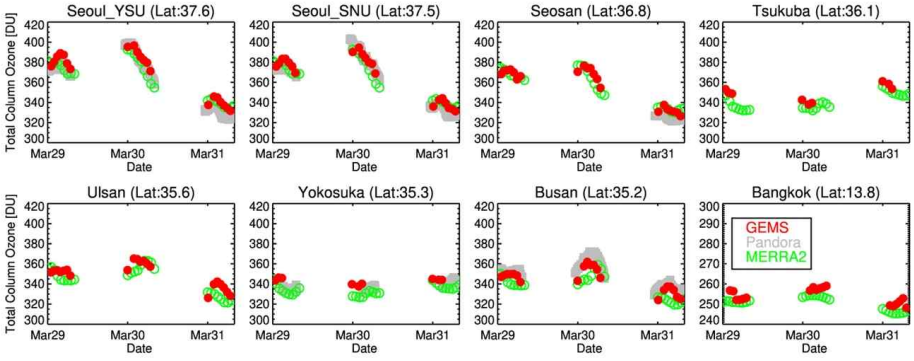

225

Figure 3. Comparison of GEMS TCO with Pandora, TROPOMI, and OMPS TCO from 29 to 31 March 2021 over eight Pandora sites.

3.2 Validation of GEMS total ozone.

230 Satellite measurements are subject to instrument measurement errors and retrieval errors from ill-posed problems. Therefore, validation is essential for scrutinizing satellite retrieval accuracy and providing confidence in the final results. The GEMS total ozone data was validated by comparing it with ground-based Pandora and other satellite measurements from OMPS and TROPOMI. For accurate validation, we used GEMS TCO between August and December 2020, a stable initial operation period with accurate Image Navigation and Registration (INR) information. The available Pandora observations during this
235 period were over Busan, Ulsan, Seoul, and Yokosuka. Table 1 presents detailed Pandora site information. Since GEMS switches to Full West mode at 13 KST in November and December, there is no GEMS measurement at Yokosuka in Japan from this time, so we used only data before this time for validation. GEMS takes 30 minutes to complete an observation over the FOR, whereas Pandora collects each measurement in 2 minutes several times per day. For temporal coincidence, we used the average of Pandora observation data before and after 15 minutes of the local GEMS observation. For spatial coincidence,
240 we used the closest GEMS data to the Pandora site. To exclude Pandora data contaminated by clouds and aerosols, we used data with the normalized root-mean-square (RMS) of weighted spectral fitting residuals less than 0.05 % and the estimated error in TCO less than 2 DU as suggested by (Tzortziou et al., 2012). We take GEMS data with a solar zenith angle of less than 75 deg. to avoid GEMS errors that may occur due to the high solar zenith angle of GEMS data.

245 **Table 1 Pandora observation sites over the GEMS comparison domain.**

Site name	Longitude	Latitude	Period

https://doi.org/10.5194/egusphere-2022-1402
Preprint. Discussion started: 21 December 2022

Busan, Korea	129.1	35.2	2020/08/01 ~ 2020/12/28
Ulsan, Korea	129.2	35.6	2020/0801 ~ 2020/1104
Seoul, Korea	127.0	37.5	2020/0818 ~ 2020/12/31
Yokosuka, Japan	139.7	35.3	2020/10/29 ~ 2020/12/31

Figure 4 represents the comparison of GEMS, TROPOMI, and OMPS with Pandora TCO at the sites. Figure 4(a) shows a high correlation of 0.91 or more with GEMS and Pandora TCO at Seoul, Busan, and Yokosuka but a low correlation of 0.83 at Ulsan, which is significantly smaller than at other sites. RMSE showed satisfactory small values, with the lowest RMSE of 2.06 DU. Positive mean biases (MBs) were observed at all sites, with the highest in August. The high correlation at Yokosuka appears due to the absence of data for August. However, the MBs showed a distinctly high value in August (summer) with 5.18% in Busan and 3.68% in Seoul, then decreased to 1.61% and -1.13% in December (winter), respectively. The MBs in Yokosuka show a slightly higher value in November and December than in October, which differs from the two stations. However, it does not seem appropriate to draw any conclusions by comparing GEMS with Yokosuka with 24 data for 5 months. Overall, it is important to note that the GEMS TCO decreases markedly over time.

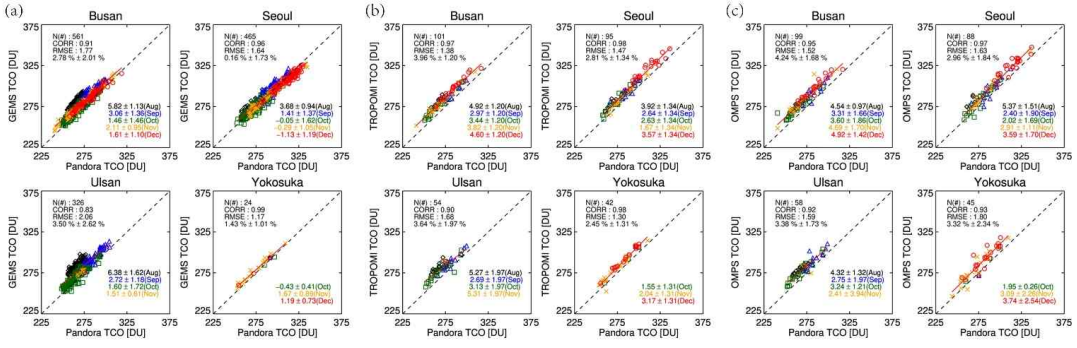

Figure 4. Scatter plots of Pandora TCO with (a) GEMS TCO, (b) TROPOMI TCO, and (c) OMPS TCO at Busan, Seoul, Ulsan, and Yokosuka. A linear fit representing a 1:1 ratio is shown in black dotted lines. The legends of N, CORR, RMSE and the number in percentage represent the number of data points, correlation coefficient, RMSE, and mean bias with standard deviation, respectively. The number on the bottom right is the percentage bias for each month

Figures 4(b) and 4(c) show the comparison of Pandora with other satellite data, OMPS and TROPOMI. Their correlation is higher than that of GEMS and Pandora. The correlation of GEMS with OMPS and TROPOMI is the lowest in Ulsan, 0.92 and

https://doi.org/10.5194/egusphere-2022-1402
Preprint. Discussion started: 21 December 2022

0.90, respectively. The RMSE between Pandora and both satellites were less than 2 DU, as in GEMS. The difference in the overall MB between GEMS and TROPMI is less than 1.2%, and that between GEMS and OMPS is less than 1.9% for the GEMS domain. Although GEMS and OMPS use the same BDM, the interesting point is that MB between these two and Pandora is as large as that of TROPOMI and Pandora. This large MB might seem to have a fundamental problem in GEMS measurement itself. We will discuss this problem in more detail at the end of this section.

Although no monthly trend was observed as distinct as GEMS, the MB in TROPOMI and OMPS increased in August (summer) and December (winter). The reason for this is that, as Herman et al., (2015) showed, the satellite retrieval methods perform temperature correction for the temperature-sensitive ozone absorption coefficient, whereas Pandora uses a fixed-temperature ozone absorption coefficient. Therefore, comparisons of satellite and Pandora data may show seasonal dependence. However, the seasonal variability shown in the comparison of GEMS and Pandora differs from those between TROPOMI (OMPS) and Pandora in magnitude and seasonal dependence.

Figure 5 is a time series showing the percentage difference between Pandora and three satellite observations, GEMS, TROPOMI, and OMPS. The overall mean bias for Pandora-TROPOMI and Pandora-OMPS is within 3.8 % for all stations, which is consistent with the previous studies (Herman et al., 2015). As for the mean standard deviation, TROPOMI has lower variability in comparison to OMPS. This could be due to the lower spatial resolution of OMPS at 50 km by 50 km compared to TROPOMI at 7.5km by 3.5 km. In the case of Ulsan, both comparisons of TROPOMI and OMPS with Pandora showed a low correlation (~0.90) and a high standard deviation (~1.8 %) compared to other stations. Even mean biases appear to be dependent on time. For example, the MB of Pandora-TROPOMI in August is observed to be ~ -6%, but the MB after September increases to -3%. These comparison results suggest the Pandora measurement at Ulsan suffers from problems in the accuracy of total ozone measurement which may be due to some form of instrument error. Therefore we have excluded the Pandora measurements at Ulsan from a reference dataset for further GEMS validation at this time.

https://doi.org/10.5194/egusphere-2022-1402
Preprint. Discussion started: 21 December 2022

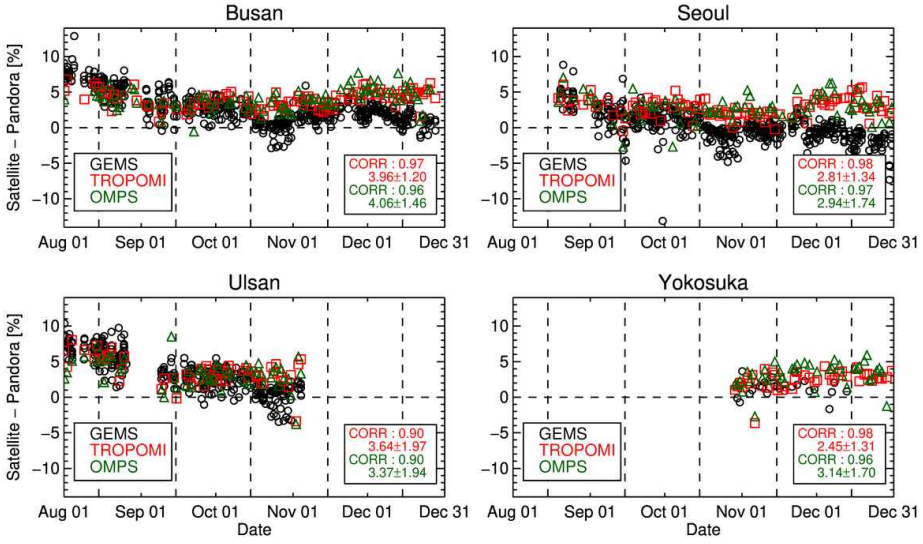

Figure 5. Time series of the daily percentage difference between Pandora and three satellite observations (with GEMS in black, TROPOMI in red and OMPS in green) at Busan, Seoul, Ulsan, and Yokosuka from August to December, 2020.

Figure 6 shows the spatial distribution of TCO from GEMS, TROPOMI, and OMPS in the GEMS domain on 30 November 2020. This figure shows that the spatial distribution of TCO observed from the three satellites is in good agreement. It shows a typical ozone distribution pattern that increases from low to high latitudes.

https://doi.org/10.5194/egusphere-2022-1402
Preprint. Discussion started: 21 December 2022

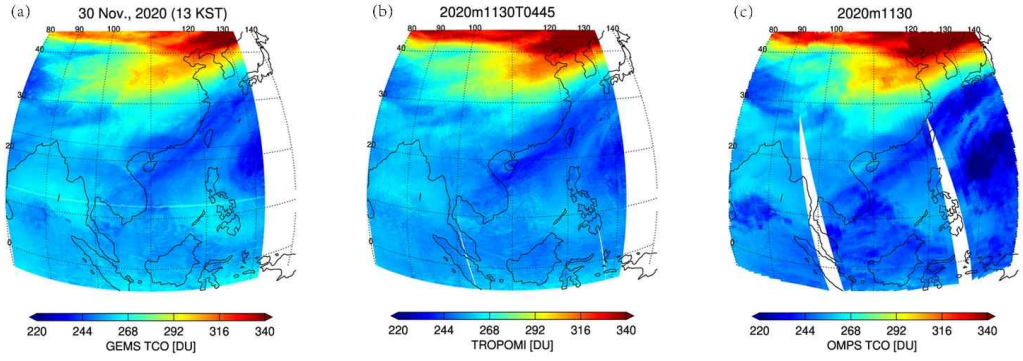

Figure 6. Maps of Total Column Ozone from (a) GEMS, (b) TROPOMI, and (c) OMPS on 30 November 2020.

295 The distribution of wave patterns at high latitudes appears to be caused by atmospheric dynamics associated with meteorological phenomena. The horizontal striping in GEMS found around 10° and 20° latitudes is an error caused by the bad pixels of the GEMS detector. These bad pixels caused the quality flag in the GEMS level 1C data to be not properly removed. Significantly lower ozone from OMPS is observed in the high reflectivity region associated with clouds shown in Figure 7. The strong anti-correlation between total ozone and cloud occurs due to the cloud height difference between actual and
300 assumed by the OMPS algorithm because the OMPS algorithm determines the cloud height from cloud climatology (Joiner and Vasilkov, 2006). This difference in cloud height affects TCO retrieval as follows. The UV measurements over the cloudy scene can provide ozone information presented in the upper part of the cloud. Only the amount of ozone present in the upper part of the cloud can be retrieved from the UV radiance measured by the satellite over the cloudy scene. The ozone produced in this case is column ozone from cloud height to the top of the atmosphere. Since ozone below the cloud cannot be observed,
305 the final TCO is calculated by adding the climatological ozone corresponding to this value's lower part of the cloud height. As shown in Figure 8, the climatology cloud height is remarkably low in the region where actual clouds exist. Therefore, since a lower cloud height is applied, the amount of ozone added below the cloud is reduced, resulting in a smaller amount of OMPS TCO.

https://doi.org/10.5194/egusphere-2022-1402
Preprint. Discussion started: 21 December 2022

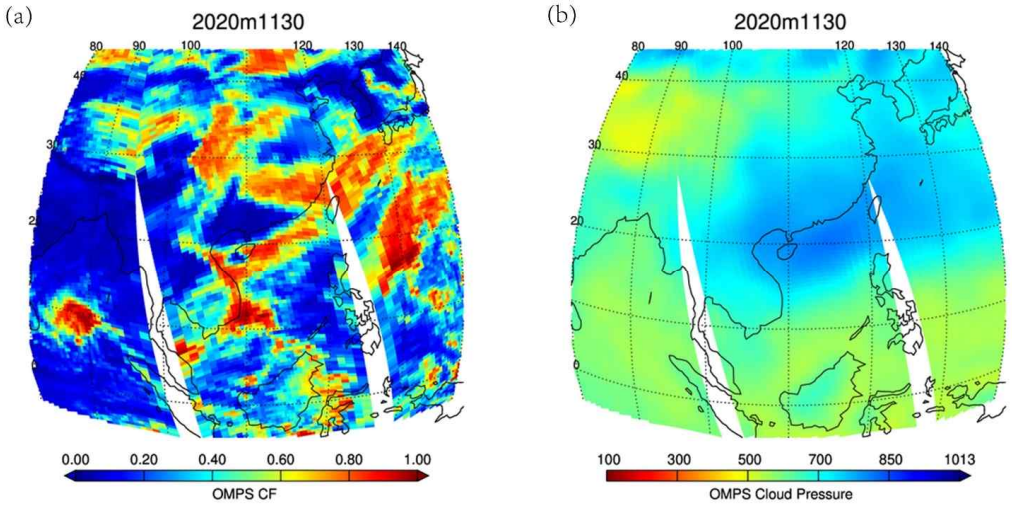

Figure 7 Maps of (a) cloud fraction (CF) and (b) cloud pressure climatology from OMPS on 30 November 2020.

The histogram analysis was performed to compare the data sets with different spatial and temporal resolutions over the GEMS domain from August to December 2020 (Figure 8). The histogram of all satellite data is similar to the normal distribution showing good agreement with each other. Especially, the distribution shape of GEMS with an average of 274.9 DU and TROPOMI with an average of 272.6 DU are very similar. However, the average of OMPS is smaller than the two satellite data, and the peak is also tilted to a lower side than the average. This appears to be due to low ozone in cloudy pixels, as mentioned earlier.

https://doi.org/10.5194/egusphere-2022-1402
Preprint. Discussion started: 21 December 2022

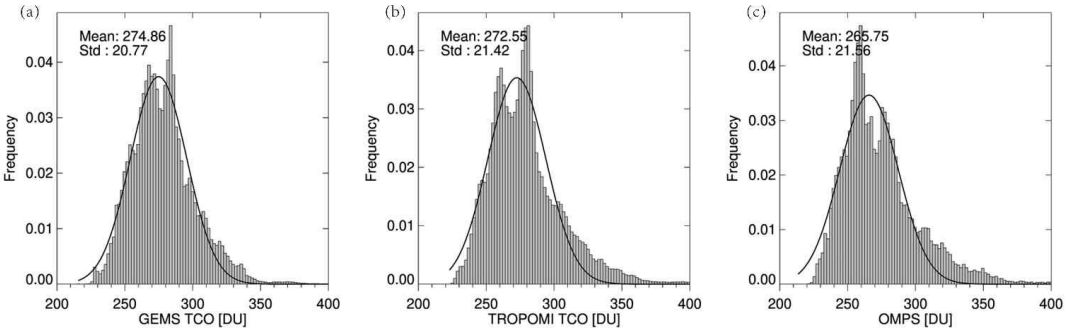

Figure 8. Histogram distribution of TCO from (a) GEMS, (b) TROPOMI, and (c) OMPS from August 01 to December 31, 2020, with their corresponding Gaussian fitting lines (black).

Since TROPOMI and OMPS have different observation times and fields of view relative to GEMS, it is necessary to match the spatial and temporal correspondence of the two data for quantitative comparison. For temporal consistency, the observation time difference between the polar orbit satellite and GEMS is less than 30 minutes. For spatial consistency, we selected the closest points within 10 km of the observation point of the two satellites. In addition, to use good quality data for comparison, we used only data satisfying the quality control conditions presented in Table 2.

Table 2. Summary of validation data and methods

	TROPOMI	**OMPS**
Validation product	GEMS total column ozone	
Validation region	East Asia (75°E - 140°E, 5°S - 45°N)	
Validation period	2020.08.01 ~ 2020.12.31	
Quality control	0 < TCO < 1008.52 180K < To3 < 260 K Ring scale factor < 0.15 -0.5 < effective albedo <1.5 CF <0.2	Quality Flag = 0, CF < 0.2 cross-track position of 1 and 35 is excluded.

https://doi.org/10.5194/egusphere-2022-1402
Preprint. Discussion started: 21 December 2022

Quality control (GEMS product)	1. cloud filtering (CF < 0.2 from GEMS L2 CLOUD product) 2. Final algorithm flag is 0 3. Exclude bad pixel.	
Co-location method	Distance difference within 10 km. Time difference < 10 min	Distance difference within 25 km. Time difference < 30 min

Figure 9 shows the quantitative comparison of GEMS TCO data with TROPOMI and OMPS TCO data for five months. It shows a high correlation coefficient greater than 0.98 and a low RMSE of less than 1.8 DU over clear sky conditions. GEMS TCO underestimates by - 0.14 % (0.42 DU) with a standard deviation of 2 % relative to TROPOMI and overestimates by + 0.1 % (0.3 DU) with a standard deviation of 2.3 % relative to OMPS. It shows that the GEMS TCO agrees very well with the TROPOMI and OMPS TCO. However, in the red circle in Figure 9(a), a distinctly high value for the GEMS TCO is observed compared to the TROPOMI TCO. The reason for this is that we did not remove the amount of SO_2 ejected by the volcanic eruption of Nishinoshima in Japan between August 1 and 5 from the GEMS TCO, which resulted in a high GEMS TCO. There will be a further discussion about this in Figure 10. Figure 9(b) shows the correlation between GEMS and OMPS. The abnormal deviation shown in Figure 9(a) was not observed. Probably, the SO_2 influence was not removed because OMPS and GEMS use a similar algorithm.

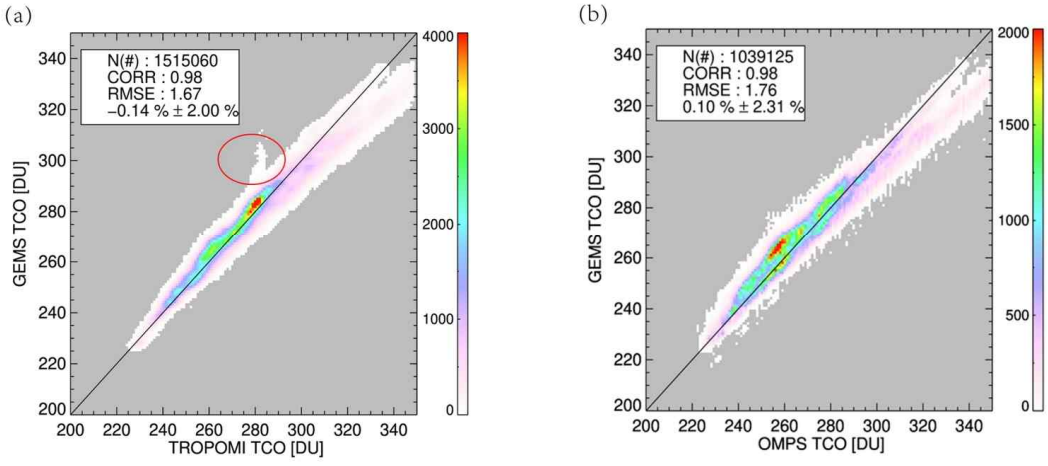

Figure 9. The comparison of GEMS TCO with (a) TROPOMI and (b) OMPS TCO from August 1 to December 31, 2020.

https://doi.org/10.5194/egusphere-2022-1402
Preprint. Discussion started: 21 December 2022

Figure 10 shows the distribution of satellite TCO and SO_2 on 4 August 2020, the day after the volcanic eruption of Nakashima in Japan. GEMS and OMPS show high TCO in regions with high SO_2 over 6 DU, but no distinctly high values from the TROPOM TCO are observed. At a wavelength of 317.5 nm, which TOMS-based GEMS and OMPS algorithms use for ozone measurement, SO_2 also has a strong absorption line. Therefore, if the SO_2 effect was not properly removed, TCO will be overestimated (Fisher et al., 2019; Krueger et al., 2008). However, since the TROPOMI direct-fitting algorithm derives the TCO using a 325-335 fitting window with a weak SO_2 absorption band, the SO_2 interference is negligible (Spurr et al., 2021).

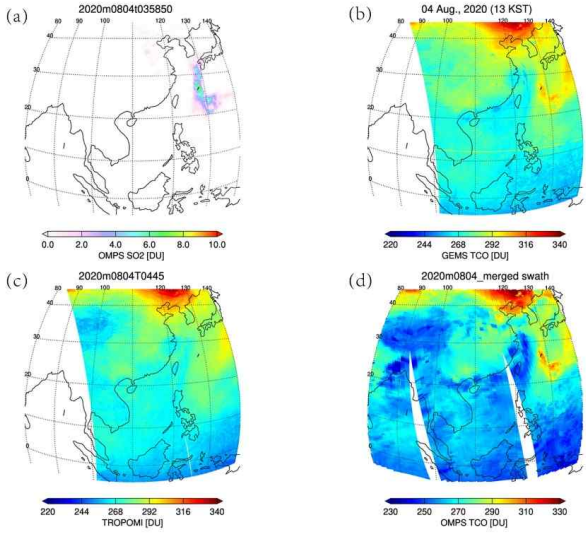

Figure 10. The map of (a) OMPS SO2, (b) GEMS TCO, (c) TROPOMI TCO, and (d) OMPS TCO in the case of the volcanic eruption of Nishinoshima on 4 August 2020.

Figure 11 shows MBs between GEMS, TROPOMI and OMPS with latitude for all months. The MBs of GEMS TCO and the TCO observed by OMPS and TROPOMI are small and positive at low latitudes, but at mid-latitudes, the MB becomes negative and tends to increase at higher latitudes. This is most dramatic at 40°N where the MB changes from + 1 % in August to - 6 % in December.

https://doi.org/10.5194/egusphere-2022-1402
Preprint. Discussion started: 21 December 2022

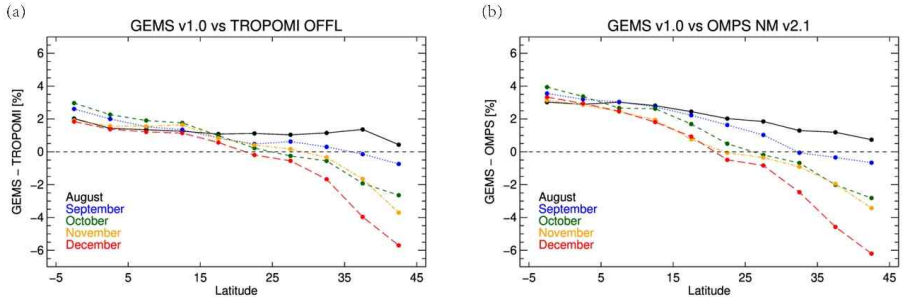

Figure 11. Mean Bias in TCO between GEMS and TROPOMI (left) and GEMS and OMPS as a function of Latitude and months from August 2020 to December 2020. GEMS retrievals with the algorithm flag equal to 0, or 1 and SZA and VZA <70°.

Kang et al. (2022) noticed a problem in GEMS Level 1C irradiance because the Bidirectional Transmittance Distribution Function (BTDF) of the GEMS diffuser changes depending on the sun illumination angle. They compared the daily GEMS irradiance to the solar reference spectrum, which was obtained from the convolution of the KNMI spectrum (Dobber et al., 2008) with the GEMS spectral response functions (SRF) (Kang et al., 2020). The GEMS irradiance was 20 % smaller than that of the reference spectrum and showed distinct spatial and seasonal variability. An empirical correction was applied to the BTDF to correct the GEMS irradiance by using the azimuthal angle and temporal variation of the GEMS instrument (Kang et al., 2022). Figure 11 shows the GEMS TCO after calculating this correction to the solar irradiance. The MB of GEMS TCO relative to OMPS and TROPOMI TCO are compared. Figure 12 shows that a reduction in MB was clearly observed at low latitudes, and nearly reaches zero. The apparent decrease seen in mid-latitudes in Figure 11 was also significantly reduced. However, the negative trend has only decreased slightly: the -6 % MB seen at 40°N in December in Figure 12 has reduced to – 4 % Judging from these differences, more study of the GEMS irradiance measurement performance is needed.

https://doi.org/10.5194/egusphere-2022-1402
Preprint. Discussion started: 21 December 2022

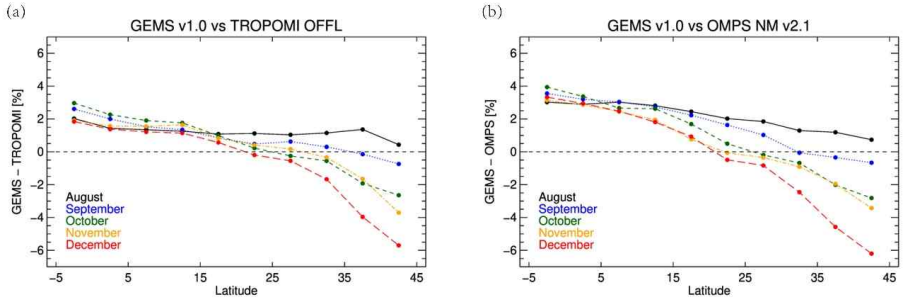

Figure 12. Mean Bias in TCO between GEMS applied BTDF correction and TROPOMI (left), and GEMS and OMPS as a function of latitude and months from August 2020 to December 2020. GEMS retrieval with the algorithm flag equal to 0 or 1, both SZA and VZA <70°.

4. Conclusion

The launch of the first geostationary environmental satellite, GEMS, has marked an important milestone in providing hourly monitoring of stratospheric ozone and air pollution, which significantly impact humans and ecosystems. This paper provides the atmospheric science community with the world's first assessment of GEMS total ozone retrieval performance and diurnal ozone variation. The algorithm used for GEMS is a more advanced version of its predecessor, the TOMS-V8 algorithm. In addition to calculating total ozone, it has the advantage of providing ozone profile and retrieval error information.

To assess the performance of the GEMS algorithm, the hourly GEMS TCO was compared with the ground-based TCO measurements from Pandora that vary considerably through the day. The diurnal variation of GEMS total ozone captures this variability and shows good agreement with that of Pandora. This indicates that the ozone undergoes significant diurnal change, primarily due to changes in stratospheric ozone, and is evidence of why hourly ozone monitoring is important to track dynamic ozone changes.

For further validation of GEMS TCO, we performed cross-comparisons between GEMS, four Pandora TCO and other satellite sensors, OMPS and TROPOMI. The correlation between Pandora and two satellite TCO datasets was slightly higher than with GEMS. All RMSE values were less than about 2 DU. All satellite TCO measurements were higher than Pandora. However, MB of GEMS showed a distinctly high value in August (summer) in Busan (5.2%) and in Seoul (3.7%), which then decreased to 1.6% and -1.1% in December (winter), respectively. In contrast, no seasonal change was observed in the MB of OMPS and TROPOMI TCO with the Pandora TCO.

The GEMS TCO agrees very well with the TROPOMI and OMPS TCO. A quantitative comparison of GEMS TCO data with TROPOMI and OMPS TCO data from August to December 2020 shows a high correlation (> 0.98) and a low RMSE (< 1.8 DU) for clear sky conditions. GEMS TCO is 0.14 % (0.42 DU) lower than TROPOMI with a standard deviation of 2 %

https://doi.org/10.5194/egusphere-2022-1402
Preprint. Discussion started: 21 December 2022

and 0.1 % (0.3 DU) higher than OMPS, with a standard deviation of 2.3 %. As MB with GEMS and Pandora showed a seasonal trend, MB with two satellites showed a latitudinal trend. The MBs of GEMS TCO and the TCO observed by the two satellites are small and positive at low latitudes, but at mid-latitudes, MB becomes negative and tends to be larger at higher latitudes. This decrease grows dramatically from August to December over which time the MB decreases to - 6% in the extreme, at 40º N.

GEMS solar irradiance is 20 % lower than the Dobber et al., (2008) reference spectrum, and shows distinct spatial and seasonal variability. A correction factor applied to GEMS removes the trend in the latitude direction of the irradiance measurement, but the seasonal tendency still remains. Judging from these differences, the calibration of the GEMS solar irradiance needs further work.

Improvements in GEMS sensor characterization should improve the quality of GEMS total ozone retrieval. Nevertheless, the results presented in this work that have been achieved thus far are a meaningful scientific advance by providing the first validated, hourly UV ozone retrievals from a satellite in geostationary orbit. This experience can be used to advance research with future geostationary environmental satellite missions, including TEMPO and Sentinel-4 which are planned to launch in 2023.

Code availability.

All input data including GEMS measurement and validation measurements related to this paper are available from the corresponding author on reasonable request (jaekim@pusan.ac.kr).

Data availability.

The GEMS total column ozone can be accessed by contacting the corresponding author (jaekim@pusan.ac.kr). TROPOMI total column ozone is available at https://tropomi.gesdisc.eosdis.nasa.gov/ (Spurr et al., 2021). OMPS total column ozone is available at https://snpp-omps.gesdisc.eosdisc.eosdis.nasa.gov/ (Flynn et al., 2014). Pandora data used in this investigation is available through the Pandonia online archive (http://data.pandonia-global-network.org/).

Author contributions

Jae Hwan Kim designed the research and managed this paper. Kanghyun Baek conducted the algorithm development and validation, and writing of the original draft. Juseon Bak contributed to the analysis of errors. David Haffner worked on the development of the GEMS algorithm. Mina Kang substantially contributed to the analysis of GEMS level-1 data. Hyunkee Hong curated a variety of data sources. All the co-authors provided comments and contributed to editing the manuscript and figures.

https://doi.org/10.5194/egusphere-2022-1402
Preprint. Discussion started: 21 December 2022

425

Competing interests.

The contact author has declared that none of the authors has any competing interests.

Special issue statement.

This article is part of the special issue "GEMS: first year in operation (AMT/ACP inter-journal SI)". It is not associated with
430 a conference.

Acknowledgements.

We thank the NASA GSFC support staff and funding for establishing and maintaining the sites of the PGN used in this investigation.

435

Financial support.

This work was supported by the National Institute of Environmental Research (NIER) of Korea (NIER-2022-04-02-036) and the National Research Foundation of Korea (NRF) grant funded by the Korea government (MSIT) (No. NRF-2020R1C1C1014522).

440

References

Ahmad, Z.: Spectral properties of backscattered UV radiation in cloudy atmospheres. J. Geophys. Res. 109, D01201. https://doi.org/10.1029/2003JD003395, 2004.
Bhartia, P., Haffner, D.: Highlights of TOMS Version 9 Total Ozone Algorithm, in: Quadrennial Ozone Symposium.
445 Toronto, Canada, 2012.
Bhartia, P.K.: OMI Algorithm Theoretical Basis Document, NASA-OMI, Washington, DC, ATBD-OMI-02, version 2.0, 2002.
Bhartia, P.K., McPeters, R.D., Mateer, C.L., Flynn, L.E., Wellemeyer, C.: Algorithm for the estimation of vertical ozone profiles from the backscattered ultraviolet technique. J. Geophys. Res. Atmos. 101, 18793–18806.
450 https://doi.org/10.1029/96JD01165, 1996.
Bovensmann, H., Burrows, J.P., Buchwitz, M., Frerick, J., Noël, S., Rozanov, V. V., Chance, K. V., Goede, A.P.H.: SCIAMACHY: Mission Objectives and Measurement Modes. J. Atmos. Sci. 56, 127–150. https://doi.org/10.1175/1520-0469(1999)056, 1999.
Brion, J., Chakir, A., Daumont, D., Malicet, J., Parisse, C.: High-resolution laboratory absorption cross section of O3.
455 Temperature effect. Chem. Phys. Lett. 213, 610–612. https://doi.org/10.1016/0009-2614(93)89169-I, 1993.
Crutzen, P.J.: THE ROLE OF NO AND N02 IN THE CHEMISTRY OF THE TROPOSPHERE AND STRA TOSPHERE, Ann. Rev. Earth Planet. Sci., 1979.

https://doi.org/10.5194/egusphere-2022-1402
Preprint. Discussion started: 21 December 2022

Daumont, D., Brion, J., Charbonnier, J., Malicet, J.: Ozone UV Spectroscopy I: Absorption Cross-Sections at Room Temperature, 1992.

Dave, J. V.: EFFECT OF AEROSOLS ON THE ESTIMATION OF TOTAL OZONE IN AN ATMOSPHERIC COLUMN FROM THE MEASUREMENTS OF ITS ULTRAVIOLET RADIANCE. J. Atmos. Sci. 35, 899–911. https://doi.org/10.1175/1520-0469, 1978.

Dave, J. V., Mateer, C.L.: A Preliminary Study on the Possibility of Estimating Total Atmospheric Ozone from Satellite Measurements. J. Atmos. Sci. 24, 414–427. https://doi.org/10.1175/1520-0469(1967), 1967.

Dobber, M., Voors, R., Dirksen, R., Kleipool, Q., Levelt, P.: The high-resolution solar reference spectrum between 250 and 550 nm and its application to measurements with the ozone monitoring instrument. Sol. Phys. 249, 281–291. https://doi.org/10.1007/s11207-008-9187-7, 2008.

Engel, A., Rigby, M., Burkholder, J.B., Fernandez, R.P., Froidevaux, L., Hall, B.D., Hossaini, R., Saito, T., Vollmer, M.K., Yao, B.: Update on Ozone-Depleting Substances (ODSs) and Other Gases of Interest to the Montreal Protocol, Global Ozone Research and Monitoring Project-Report, 2018.

Fisher, B.L., Krotkov, N.A., Bhartia, P.K., Li, C., Carn, S.A., Hughes, E., Leonard, P.J.T.: A new discrete wavelength backscattered ultraviolet algorithm for consistent volcanic SO2 retrievals from multiple satellite missions. Atmos. Meas. Tech. 12, 5137–5153. https://doi.org/10.5194/amt-12-5137-2019, 2019.

Fishman, J., Bowman, K.W., Burrows, J.P., Richter, A., Chance, K. V., Edwards, D.P., Martin, R. V., Morris, G.A., Pierce, R.B., Ziemke, J.R., Al-Saadi, J.A., Creilson, J.K., Schaack, T.K., Thompson, A.M.: Remote Sensing of Tropospheric Pollution from Space. Bull. Am. Meteorol. Soc. 89, 805–822. https://doi.org/10.1175/2008BAMS2526.1, 2008.

Fishman, J., Larsen, J.C.: Distribution of total ozone and stratospheric ozone in the tropics: implications for the distribution of tropospheric ozone. J. Geophys. Res. 92, 6627–6634. https://doi.org/10.1029/JD092ID06P06627, 1987.

Flynn, L., Long, C., Wu, X., Evans, R., Beck, C.T., Petropavlovskikh, I., McConville, G., Yu, W., Zhang, Z., Niu, J., Beach, E., Hao, Y., Pan, C., Sen, B., Novicki, M., Zhou, S., Seftor, C.: Performance of the Ozone Mapping and Profiler Suite (OMPS) products. J. Geophys. Res. Atmos. 119, 6181–6195. https://doi.org/10.1002/2013JD020467, 2014.

Haffner, D.P., McPeters, R.D., Bhartia, P.K., Labow, G.J., Haffner, D.P., McPeters, R.D., Bhartia, P.K., Labow, G.J.: The TOMS V9 Algorithm for OMPS Nadir Mapper Total Ozone: An Enhanced Design That Ensures Data Continuity, in: AGU Fall Metting. San Francisco, CA, United States, 2015.

Haffner, D.P et al.: Total Ozone Mapping Spectrometer (TOMS) Version 9 Algorithm, Manuscript in preparation. Manuscript in preparation, 2022.

Herman, J., Evans, R., Cede, A., Abuhassan, N., Petropavlovskikh, I., McConville, G.: Comparison of ozone retrievals from the Pandora spectrometer system and Dobson spectrophotometer in Boulder, Colorado. Atmos. Meas. Tech. 8, 3407–3418. https://doi.org/10.5194/amt-8-3407-2015, 2015.

Ingmann, P., Veihelmann, B., Langen, J., Lamarre, D., Stark, H., Courrèges-Lacoste, G.B.: Requirements for the GMES Atmosphere Service and ESA's implementation concept: Sentinels-4/-5 and -5p. Remote Sens. Environ. 120, 58–69. https://doi.org/10.1016/J.RSE.2012.01.023, 2012.

Jacob, D.J., Logan, J.A., Murti, P.P.: Effect of rising Asian emissions on surface ozone in the United States, JULY. American Geophysical Union. https://doi.org/10.1029/1999GL900450, 1999.

Joiner, J., Vasilkov, A.P.: First results from the OMI rotational raman scattering cloud pressure algorithm. IEEE Trans. Geosci. Remote Sens. 44, 1272–1281. https://doi.org/10.1109/TGRS.2005.861385, 2006.

Kang, M., Ahn, M.H., Liu, X., Jeong, U., Kim, J.: Spectral calibration algorithm for the geostationary environment monitoring spectrometer (Gems). Remote Sens. 12, 1–17. https://doi.org/10.3390/rs12172846, 2020.

Kang, M et al.: On-Orbit Calibration of Bi-directional Transmittance Distribution Function (BTDF) for Geostationary Environment Monitoring Spectrometer (GEMS). Manuscript in preparation, 2022.

Kim, J., Jeong, U., Ahn, M.H., Kim, J.H., Park, R.J., Lee, Hanlim, Song, C.H., Choi, Y.S., Lee, K.H., Yoo, J.M., Jeong, M.J., Park, S.K., Lee, K.M., Song, C.K., Kim, Sang Woo, Kim, Y.J., Kim, Si Wan, Kim, M., Go, S., Liu, X., Chance, K., Miller, C.C., Al-Saadi, J., Veihelmann, B., Bhartia, P.K., Torres, O., Abad, G.G., Haffner, D.P., Ko, D.H., Lee, S.H., Woo, J.H., Chong, H., Park, S.S., Nicks, D., Choi, W.J., Moon, K.J., Cho, A., Yoon, J., Kim, S. kyun, Hong, H., Lee, K., Lee, Hana, Lee, S., Choi, M., Veefkind, P., Levelt, P.F., Edwards, D.P., Kang, M., Eo, M., Bak, J., Baek, K., Kwon, H.A., Yang, J., Park, J., Han, K.M., Kim, B.R., Shin, H.W., Choi, H., Lee, E., Chong, J., Cha, Y., Koo, J.H., Irie, H., Hayashida, S., Kasai, Y., Kanaya, Y., Liu, C., Lin, J., Crawford, J.H., Carmichael, G.R., Newchurch, M.J.,

https://doi.org/10.5194/egusphere-2022-1402
Preprint. Discussion started: 21 December 2022

Lefer, B.L., Herman, J.R., Swap, R.J., Lau, A.K.H., Kurosu, T.P., Jaross, G., Ahlers, B., Dobber, M., McElroy, C.T., Choi, Y.: New era of air quality monitoring from space: Geostationary environment monitoring spectrometer (GEMS). Bull. Am. Meteorol. Soc. 101, E1–E22. https://doi.org/10.1175/BAMS-D-18-0013.1, 2020.

Klenk, K.F., Bhartia, P.K., FLEIG, A.J., Kaveeshwar, V.G., McPeters, R.D., Smith, P.M.: Total ozone determination from the BUV experiment. J. Appl. Meteorol. 21, 1672–1684, 1982.

Krueger, A., Krotkov, N., Carn, S.: El Chichon: The genesis of volcanic sulfur dioxide monitoring from space. J. Volcanol. Geotherm. Res. 175, 408–414. https://doi.org/10.1016/J.JVOLGEORES.2008.02.026, 2008.

Levelt, P.F., Van Den Oord, G.H.J., Dobber, M.R., Mälkki, A., Visser, H., De Vries, J., Stammes, P., Lundell, J.O.V., Saari, H.: The ozone monitoring instrument. IEEE Trans. Geosci. Remote Sens. 44, 1093–1100. https://doi.org/10.1109/TGRS.2006.872333, 2006.

Malicet, J., Daumont, D., Charbonnier, J., Parisse, C., Chakir, A., Brion, J.: Ozone UV spectroscopy. II. Absorption cross-sections and temperature dependence. J. Atmos. Chem. 1995 213 21, 263–273. https://doi.org/10.1007/BF00696758, 1995.

Mcpeters, R.D., Bhartia, P.K., Krueger, A.J., Herman, J.R., Schlesinger, B.M., Wellemeyer, C.G., Seftor, C.J., Jaross, G., Taylor, S.L., Swissler, T., Torres, O., Labow, G., Byerly, W., Cebula, R.P.: Nimbus-7 Total Ozone Mapping Spectrometer (TOMS) Data Products User's Guide, NASA Reference Publication 1384, Washington, DC, 1996.

McPeters, R.D., Labow, G.J.: Climatology 2011: An MLS and sonde derived ozone climatology for satellite retrieval algorithms. J. Geophys. Res. Atmos. 117. https://doi.org/10.1029/2011JD017006, 2012.

National Institute of Environmental Research (NIER): GEMS Level-1 User Guide V1.0, Incheon, Republic of Korea, Environmetal Satellite Center, https://nesc.nier.go.kr/product/document?page=1&limit=10 (accessed 10.25.22) , 2020.

Scientific Assessment of Ozone Depletion: Global Ozone Research and Monitoring Project Report No. 55 World Meteorological Organization (2015). URL https://public.wmo.int/en/media/news/scientific-assessment-of-ozone-depletion-published (accessed 3.25.21), 2014.

Spurr, R.: LIDORT and VLIDORT: Linearized pseudo-spherical scalar and vector discrete ordinate radiative transfer models for use in remote sensing retrieval problems, in: Light Scattering Reviews 3. Springer Berlin Heidelberg, pp. 229–275. https://doi.org/10.1007/978-3-540-48546-9_7, 2008.

Spurr, R., Loyola, D., Roozendael, M. Van, Lerot, C.: S5P / TROPOMI Total Ozone ATBD. Dtsch. Zent. für Luft und Raumfahrt 67, 2021.

Tzortziou, M., Herman, J.R., Cede, A., Abuhassan, N.: High precision, absolute total column ozone measurements from the Pandora spectrometer system: Comparisons with data from a Brewer double monochromator and Aura OMI. J. Geophys. Res. Atmos. 117. https://doi.org/10.1029/2012JD017814, 2012.

Veefkind, J.P., Aben, I., McMullan, K., Förster, H., de Vries, J., Otter, G., Claas, J., Eskes, H.J., de Haan, J.F., Kleipool, Q., van Weele, M., Hasekamp, O., Hoogeveen, R., Landgraf, J., Snel, R., Tol, P., Ingmann, P., Voors, R., Kruizinga, B., Vink, R., Visser, H., Levelt, P.F.: TROPOMI on the ESA Sentinel-5 Precursor: A GMES mission for global observations of the atmospheric composition for climate, air quality and ozone layer applications. Remote Sens. Environ. 120, 70–83. https://doi.org/10.1016/J.RSE.2011.09.027, 2012.

Wellemeyer, C.G., Taylor, S.L., Seftor, C.J., McPeters, R.D., Bhartia, P.K.: A correction for total ozone mapping spectrometer profile shape errors at high latitude. J. Geophys. Res. Atmos. 102, 9029–9038. https://doi.org/10.1029/96JD03965, 1997.

Zoogman, P., Liu, X., Suleiman, R.M., Pennington, W.F., Flittner, D.E., Al-Saadi, J.A., Hilton, B.B., Nicks, D.K., Newchurch, M.J., Carr, J.L., Janz, S.J., Andraschko, M.R., Arola, A., Baker, B.D., Canova, B.P., Chan Miller, C., Cohen, R.C., Davis, J.E., Dussault, M.E., Edwards, D.P., Fishman, J., Ghulam, A., González Abad, G., Grutter, M., Herman, J.R., Houck, J., Jacob, D.J., Joiner, J., Kerridge, B.J., Kim, J., Krotkov, N.A., Lamsal, L., Li, C., Lindfors, A., Martin, R. V., McElroy, C.T., McLinden, C., Natraj, V., Neil, D.O., Nowlan, C.R., O'Sullivan, E.J., Palmer, P.I., Pierce, R.B., Pippin, M.R., Saiz-Lopez, A., Spurr, R.J.D., Szykman, J.J., Torres, O., Veefkind, J.P., Veihelmann, B., Wang, H., Wang, J., Chance, K.: Tropospheric emissions: Monitoring of pollution (TEMPO). J. Quant. Spectrosc. Radiat. Transf. 186, 17–39. https://doi.org/10.1016/J.JQSRT.2016.05.008, 2017.